Construction and Building Materials 346 (2022) 128459

Contents lists available at ScienceDirect

Construction and Building Materials

journal homepage: www.elsevier.com/locate/conbuildmat

Optimization of matrix viscosity improves polypropylene fiber dispersion and properties of engineered cementitious composites

Duo Zhang [a], He Zhu [a], Menjun Hou [a], Kimberly E. Kurtis [b], Paulo J.M. Monteiro [c], Victor C. Li [a,*]

[a] Department of Civil and Environmental Engineering, University of Michigan, 2350 Hayward Street, Ann Arbor, MI 48109, United States
[b] School of Civil and Environmental Engineering, Georgia Tech, 790 Atlantic Dr., Atlanta, GA 30332, United States
[c] Department of Civil and Environmental Engineering, University of California, Berkeley, CA 94720, United States

ARTICLE INFO

Keywords:
Engineered Cementitious Composites (ECC)
Polypropylene (PP) fiber
Fiber dispersion
Tensile ductility
Calcined clay

ABSTRACT

Engineered cementitious composites (ECC) is a durable cementitious material with high tensile ductility and strain-hardening characteristics. Although considered as a cost-effective fiber for ECC, polypropylene (PP) fiber is reportedly difficult to disperse in mortar matrix due to its high aspect ratio and hydrophobicity. In this study, the matrix viscosity of a low-carbon ECC based on limestone calcined clay cement was tailored as a variable to improve PP fiber dispersion under a pre-determined mixing protocol. The effect of matrix viscosity on the composite fresh and hardened properties was investigated experimentally. Results suggested an optimal range of matrix viscosity (10.3–11.5 Pa·s) favors the composite tensile strength and strain capacity at 28 days. At the optimal state with a 0.1 % viscosity modifying admixture (VMA)-to-binder mass ratio, PP-ECC achieved 7.0 % tensile strain capacity and 3.5 MPa ultimate tensile strength. When matrix viscosity falls outside the desired range, both ultimate tensile strength and strain capacity were diminished. By tailoring the VMA dosage, the matrix viscosity can be adjusted for desired fiber dispersion, workability, and mechanical properties. The findings of this study provide a technical reference for the practical design and application of PP-ECC.

1. Introduction

Engineered Cementitious Composites (ECC) is an ultra-ductile class of fiber-reinforced cementitious composite (FRCC) [1]. Typical ECCs develop tensile strain capacities higher than 3 %, i.e., over 300 times that of conventional concrete [2]. Under uniaxial tension, ECC forms multiple fine cracks by increasing the number of cracks instead of crack width. The tight cracks (typically below 100 μm in width) continue carrying load via microfiber bridging [3,4]. This intrinsic capability of crack width control limits material permeability in loaded conditions even beyond the elastic state [5,6] and improves material self-healing [7–9] and structural durability [10–13].

The material design of ECC is established on the micromechanical principles by tailoring the properties of the matrix, fiber, and fiber/matrix interface [14–16]. Although the high tensile ductility and robust crack width control can be achieved in the design phase, the actual material processing often leads to high variability in these properties. A potential source of this variability is the fiber distribution in the cementitious matrix. Li and Li [17] addressed the impact of PVA fiber dispersion on ECC's tensile ductility and established the relationship among the matrix viscosity, fiber dispersion uniformity, and ECC tensile strain capacity. The study suggested a strong dependency of the magnitude and variability of PVA-ECC tensile ductility on the fiber distribution, where a poor fiber distribution reduces the fiber volume at the weakest cross-section, thus lowering the fiber bridging capability [17]. As a result, the composite strain-hardening process may be interrupted, causing premature tensile failure that limits the ultimate tensile strength and strain capacity. In this scenario, full multiple microcrack saturation may be hindered.

It is proposed that the viscosity of the mortar matrix could tailor the fiber dispersion. Similar findings on polymeric fiber dispersion were reported in FRCC. Si et al., [18] found that the hardened property of PVA-FRCC can vary significantly with the rheological property due to the variation of fiber dispersion. Cao et al., [19] evaluated the relationship between the FRCC rheology, PVA fiber dispersion, and composite strength, and found that a good fiber dispersion minimizes flaw size and increases fiber bridging capability at the weakest location.

Among common polymeric fibers used in ECC, polypropylene (PP) fiber has a relatively low cost and is attractive for large-scale applications. PP fiber has been successfully used in ECC. By tailoring the

* Corresponding author.
E-mail address: vcli@umich.edu (V.C. Li).

https://doi.org/10.1016/j.conbuildmat.2022.128459
Received 10 April 2022; Received in revised form 4 July 2022; Accepted 9 July 2022
Available online 14 July 2022

micromechanical design, Yang [20] incorporated a high-tenacity (defined as the fiber breaking force divided by the linear mass density, i.e., denier) PP (HTPP) fiber into ECC and achieved a tensile strain capacity of up to 4 % and an ultimate tensile strength up to 2.5 MPa. Felekoglu et al., [21] investigated the impact of matrix flowability, mixing procedure, and curing conditions on the tensile property of HTPP-ECC. It was suggested that a certain range of matrix flowability is required to achieve robust tensile ductility for HTPP-ECC. The mixing of PP fiber was reportedly difficult due to the relatively high aspect ratio (i.e., length/diameter ratio, ~1000) compared to that of PVA fibers (~205). The high aspect ratio is necessary for effective microfiber bridging due to the low fiber/matrix interfacial bond in hydrophobic fibers such as PP. By adjusting the matrix flowability and curing conditions, Felekoglu et al., [21] developed a moderate-strength HTPP-ECC with a tensile ductility of 1.91–3.91 % and compressive strength of 30–70 MPa at 28 days. It was also reported that a high matrix viscosity could result in a poor fiber distribution for PP-ECC [22].

Limestone calcined clay cement (LC3) has received increasing attention for its low environmental footprint and enhanced durability [23,24]. The coupled use of limestone and calcined kaolinite-containing clays, where kaolinite comprises at least 40 % of the clay, enables a high clinker substitution as an efficient pozzolan [25]. LC3 has been incorporated into PP-ECC, leading to a tensile strain capacity of up to 6 % and an ultimate tensile strength of 2.5–4.8 MPa [26]. The LC3-PP-ECC shows robust self-healing capability and crack control (below 82 μm) while reducing 48 % carbon footprint compared to conventional ECC based on Portland cement. Liu et al., [27] studied the mechanical behavior of LC3-PP-ECC and found that compressive strength decreased substantially with an increasing PP fiber content due to the internal defects and flaws led by the fiber incorporation. LC3 has different rheology from conventional Portland cement. The mortar and concrete made with LC3 show reduced workability, higher demand for superplasticizer, and lower slump retention over time [28–30]. The rheological distinction between LC3 and conventional Portland cement binders has not been previously considered in designing PP-ECC to enhance fiber bridging efficiency.

While the relations among matrix rheology, PVA fiber dispersion, and ECC composite properties have been well established, such relations for ECC reinforced with high aspect ratio hydrophobic PP fibers remain unclear. As PP fibers are low-cost but difficult to disperse, clarifying these relations for PP-ECC is critical to the material design and quality control and may accelerate ECC's tech-to-market transitions to realize lifecycle emission reduction. In this regard, the present study aims to elucidate the effect of matrix rheology on PP fiber dispersion and to correlate the matrix plastic viscosity to the composite fresh and mechanical properties. Moreover, an optimal range of matrix viscosity controlled by the dosage of viscosity modifying admixture was identified for PP-ECC. The findings of this study would improve the quality control of low-carbon, low-cost ECC associated with the fiber dispersion process and may serve as a technical reference for field practice.

2. Experimental program

2.1. Materials, mix design, and mixing protocol

The binder materials include ASTM Type I Ordinary Portland cement (OPC), Class C fly ash, metakaolin (Imerys), and limestone (Imerys). F75 silica sand (US Silica) was used as a fine aggregate. Hydroxypropyl methylcellulose (HPMC, Acros Organics) was added for rheology control, and a high range water reducing admixture (HRWRA, MasterGlenium 7920) was used for workability. Chopped PP fiber from Saint-Gobain was used. The technical specification of PP fiber is shown in Table 1.

Table 2 shows two ECC mix designs used in this study, including Mix A without the sand incorporation and Mix B with a sand-to-cement mass ratio of 1:1. The binder composition is identical for Mix A and Mix B, and PP fiber was added at 2 % by ECC volume. The SP dosage was 0.8 % by mass of the cementitious material for Mix A and 0.6 % for Mix B to maintain the same ECC slump flow diameter for consistent workability.

Table 1
Technical property of PP fiber.

Diameter	Length	Nominal strength	Young's modulus	Elongation
μm	mm	MPa	GPa	%
12	12	910	9	22

Table 2
ECC mix proportion (mass ratio).

Composition	Mix A	Mix B
Portland Cement	1	1
Fly Ash	2	2
Metakaolin	0.5	0.5
Limestone	0.5	0.5
Silica Sand	–	1
Water	1	1
PP Fiber, vol%	2	2

Note: HRWRA was added at 0.6% by binder mass for Mix A and 0.8% by binder mass for Mix B; HPMC was added at 0%, 0.025%, 0.05%, 0.1%, 0.15%, and 0.2% by binder mass for both mixes.

A Hobart mortar mixer was used for ECC mixing. The mixing protocol followed three steps: 1) at low speed, all solid ingredients were mixed for 4 min, including cement, limestone, metakaolin, fly ash, HPMC, and silica sand if applicable, 2) water mixed with HRWRA was added and mixed at low speed for 6 min, 3) PP fibers were added and mixed at low speed for 2 min, and 4) the mixture was finalized at medium speed for additional 2 min.

2.2. Rheology measurement

The fresh matrix property was evaluated before adding fibers. Due to the use of sand in ECC mixes, a concrete rheometer was selected as opposed to the one used for cement pastes. An ICAR Plus Rheometer (Germann Instruments) with a continuous torque range of 0.01–32 N·m was used to characterize the matrix rheology. Similar to concrete, a fresh mortar matrix flows under the action of shear stresses. Its flow behavior can be described by the Bingham model represented in **Eq. (1)**.

$$\tau = \tau_0 + \mu\dot{\gamma} \tag{1}$$

where τ_0 is the yield stress (Pa), μ is the plastic viscosity (Pa·s), and $\dot{\gamma}$ is the shear strain rate (1/s).

The ICAR Plus is a vane-type rheometer with a vane diameter of 127 mm and a vane height of 127 mm. During measurements, the vane was set to rotate at multiple speeds following the protocol shown in Fig. 1 to generate the respective shear strain rates $\dot{\gamma}$ (**Eq. (2)**) in the mixture. The torques applied to the vane were recorded and converted to shear stresses τ. Following **Eq. (1)**, linear regression can be adopted to describe the relation between shear strain rate $\dot{\gamma}$ and shear stress τ and to determine the plastic viscosity μ. As shown in Fig. 1, to break down the static condition formed by the matrix thixotropic behavior, an initial

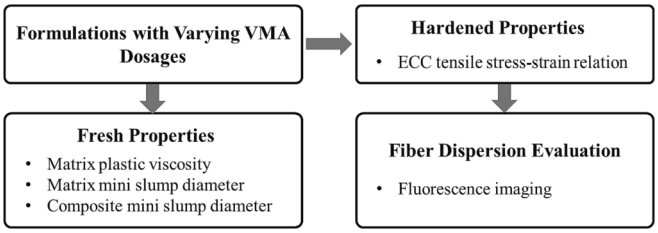

Fig. 1. Experimental program.

stage at a 0.5 rps speed was applied for 60 s. The vane subsequently slowed down at a step size of 0.05 rps and 5 s until reaching a final speed of 0.05 rps. The torque measured under this protocol was converted into shear stress and plotted as a function of shear strain rate. For each mixture, the measurement was repeated three times, and the average was reported. Fig. 2 shows an example of matrix rheology test results. The minimum R^2 values were found to be 0.97 for all mixes examined here, indicating a strong linear correlation between the shear stresses and shear strain rates.

$$\dot{\gamma} = \frac{Revolutionpersecond(rps) \times 2\pi r_0}{r_1 - r_0} \tag{2}$$

where r_0 and r_1 are the radii of vane and container, respectively.

Apart from the rheology test, the ASTM C230 flow table test was a fast and straightforward method for evaluating the matrix's fresh property. Fig. 3 shows the test schematic. The test was conducted before and after the fiber addition to assess the impact of PP fiber addition on the flowability. The deformability factor Γ is determined in **Eq. (3)** [31].

$$\Gamma = \frac{(D_1 - D_0)}{D_0} \tag{3}$$

where Γ is the fresh mixture (mortar matrix or ECC) deformability factor; D_1 is the average of d_1, d_2, and d_3; D_0 is the diameter of the bottom of the slump cone, i.e., 100 mm.

2.3. ECC uniaxial tension test

A separate group of ECC was mixed using the same mix designs and then cast into steel molds to form the specimens shown in Fig. 4. The samples were demolded after 1 day and subsequently cured for 27 days. An Instron loading frame was used for the direct tension test at a constant rate of 0.5 mm/min. Two Linear Variable Differential Transformers (LVDT) were used to capture the elongation in the center 80-mm gauge section during the loading process.

2.4. Fiber dispersion

To determine the fiber distribution on an ECC cross-section, fluorescence microscopy was used to create a contrast between the PP fibers and cementitious matrix, such that the number and location of fibers could be identified by image analysis. Organic materials, such as PP, are fluorescent under ultraviolet (UV) light excitation, whereas the cementitious matrix mostly remains dark under UV light [32]. Fig. 4 shows an example microscopic image of an ECC section under UV light. The PP fibers with a diameter of 12 μm can be distinguished clearly from the relatively dark cementitious background.

As shown in Fig. 4, a 5-mm thick piece was cut near the fractured section of the dogbone-shaped ECC specimen. The fractured section is the weakest plane of each specimen and reflects the lowest fiber dispersion, which was compared among various mix designs and VMA dosages. The sliced sample was then polished with isopropanol on the cut surface to enhance the image quality. A Nikon E800 microscopy was adopted for image collection. A mercury lamp generated UV light, and the light emitted from the sample surface was captured by a CCD camera [17]. Fluorescent images were taken at 2 × magnification and stitched together to attain the full view of a sample cross-section.

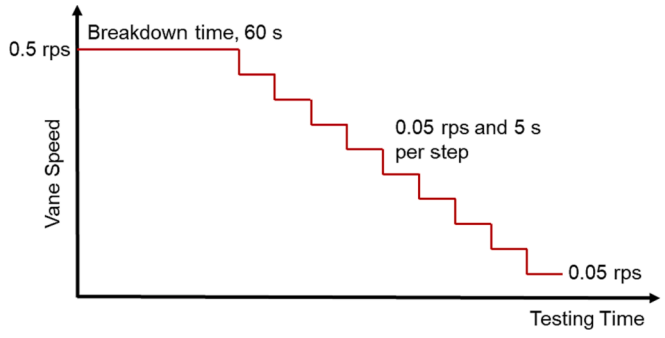

Fig. 2. Rheology testing protocol.

To exclude the wall effect (at molding surface) and the impact of surface finishing on the result of fiber dispersion, a 20-by-10 mm center section out of the 30 × 13 mm cross-section was sampled for observation. Raw images were first smoothened with Gaussian filter to reduce noises and then binarized by global thresholding based on the image histogram. The Otsu algorithm was adopted for binarizing. The 20 mm × 10 mm observation field was divided equally into 128 unit areas. As an estimate, the objects formed by pixels were counted as the number of fibers over each area, and the objects that may combine multiple fibers were considered as one fiber.

The degree to which random discontinuous fibers are distributed in a uniform matrix can be quantified by the fiber dispersion coefficient α as shown in **Eqs. 4–5** [17,33].

$$\Psi(x) = \sqrt{\frac{\sum (x_i - \overline{x})^2}{n}} / \overline{x} \tag{4}$$

$$\alpha = e^{[-\Psi(x)]} \tag{5}$$

where.

x_i is the number of fibers in the i^{th} unit area;

$\overline{x}$ is the average number of fibers per unit area, obtained from $\overline{x} = \left(\sum_{i=1}^{n} x_i\right)/n$;

n is the total number of unit area;

$\Psi(x)$ is the coefficient of variation of the number of fibers in each unit area;

α is the fiber dispersion coefficient and varies between 0 and 1.

Eqs. 4–5 suggest that the physical meaning of α is the natural exponential function of the negative coefficient of variation of the number of fibers across various unit areas, which was determined from the fiber distribution pattern shown on fluorescence images. $\alpha = 1$ indicates uniform fiber dispersion, whereas α approaches 0 when the coefficient of variation becomes large.

3. Results and discussion

3.1. Matrix rheological properties

The rheology test results indicate that incorporating HPMC (as a VMA) changes the matrix viscosity substantially, with up to a fivefold increase over the dosage range examined. Fig. 5 plots the relationships between the matrix plastic viscosity and VMA content, which appear to be linear for both mixes. HPMC was reported to thicken the mortar mixes by promoting cohesion among cementitious particles in the fresh state [34,35], and a higher HPMC molecular weight strengthens the thickening effect and improves water retention [36]. Relative to Mix A (without sand), the incorporation of silica sand into Mix B lowered the matrix plastic viscosity. The viscosity loss in the presence of silica sand can be attributed to the diluted binder content and the simultaneously increased inter-particle distance caused by the fine aggregate incorporation [37].

Similar to the plastic viscosity, the matrix dynamic yield stress strongly correlates with the VMA content up to 0.2 % by binder mass. As shown in Fig. 6, the matrix dynamic yield stress increased from 23.1 Pa to 135.4 Pa for Mix A and from 0.57 Pa to 88.7 Pa for Mix B, as the VMA content increased from 0 to 0.2 %. When incorporating HPMC into a cement paste, the dynamic yield stress generally increases with the plastic viscosity due to the increased formation of agglomerates and connected particles [38]. This may generate a negative influence on the composite workability.

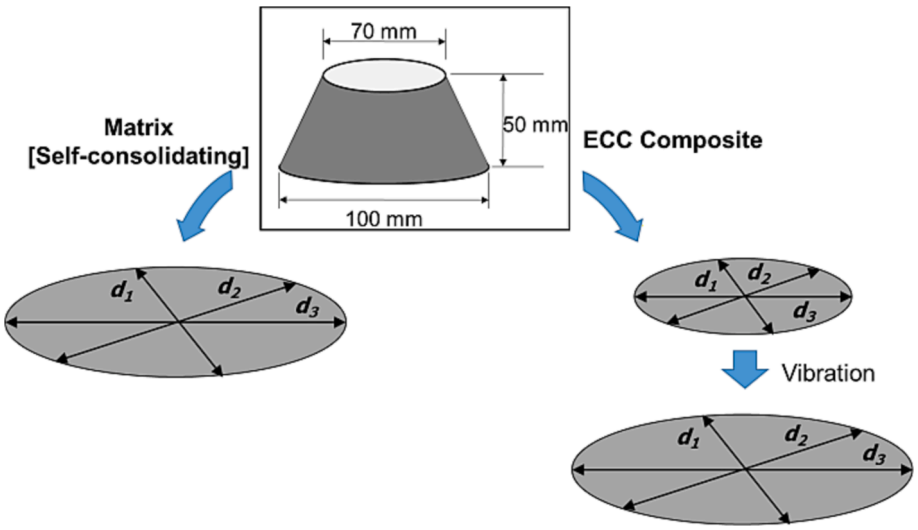

Fig. 3. Flow table test schematic.

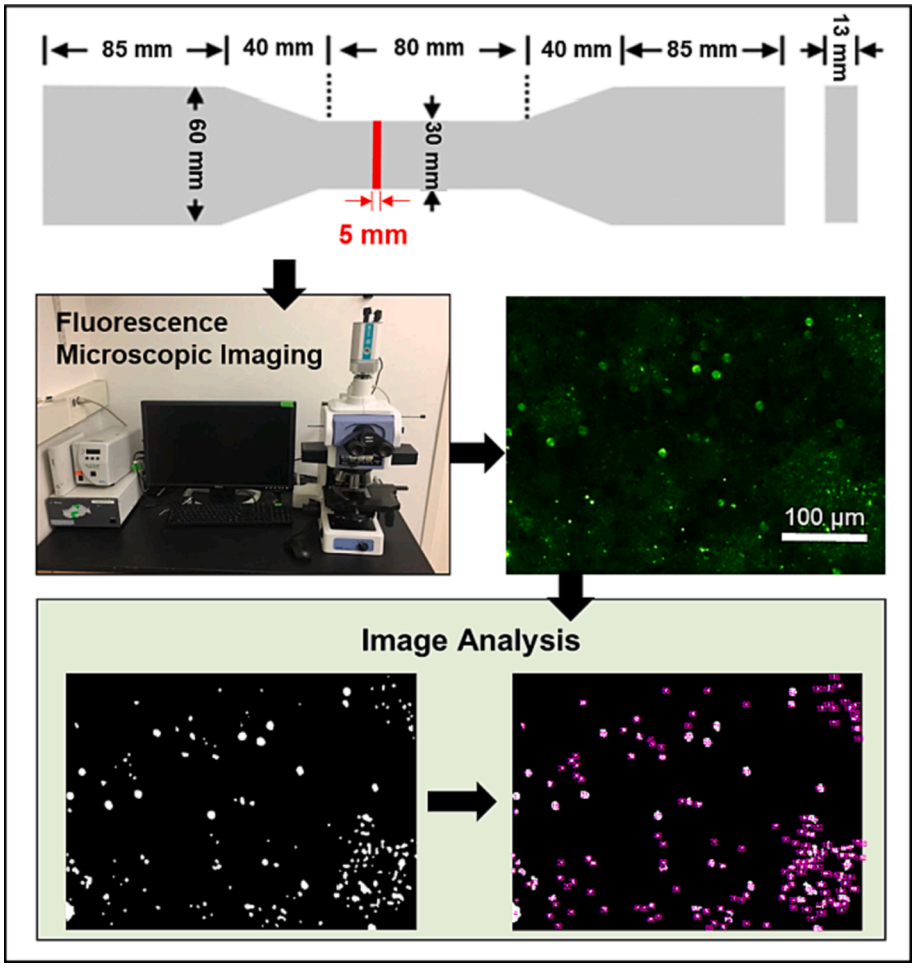

Fig. 4. ECC Fiber dispersion characterization schematic.

The deformation factor Γ serves as a simple indicator of the fresh matrix property. Figs. 7-8 correlate the deformation factor to the VMA content and matrix viscosity, respectively. A linear relationship was found between the VMA content and deformation factor, with R^2 above 0.95 for both mixes, while the matrix viscosity and deformation factor seemingly fit into a parabolic relationship. HPMC was reported to counteract the effect of PCE superplasticizer by chelating Ca^{2+} into agglomerates and precipitates [39]. It also reduces PCE's dispersion by competitive adsorption [40]. This inevitable competitive effect accounts for the lowered flowability for cement mortars plasticized with PCE admixture.

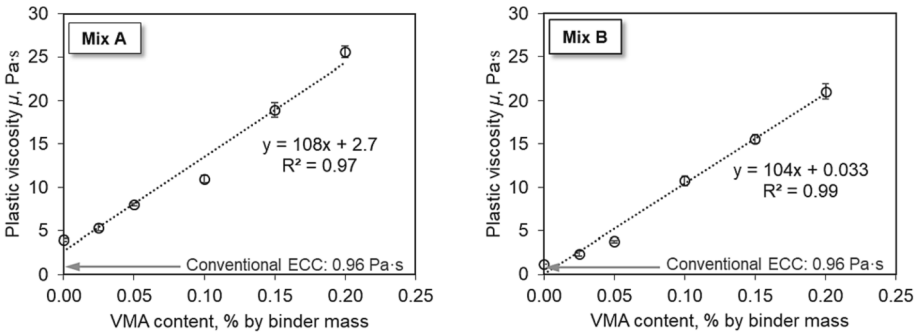

Fig. 5. Matrix plastic viscosity at various VMA contents. Note: Conventional ECC has an OPC-to-fly ash mass ratio of 2 and has no metakaolin or limestone.

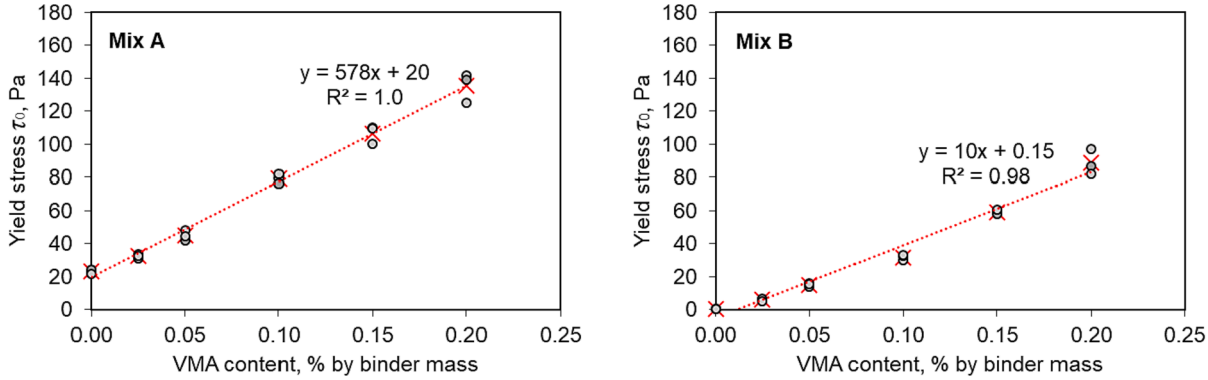

Fig. 6. Matrix dynamic yield stress at various VMA contents.

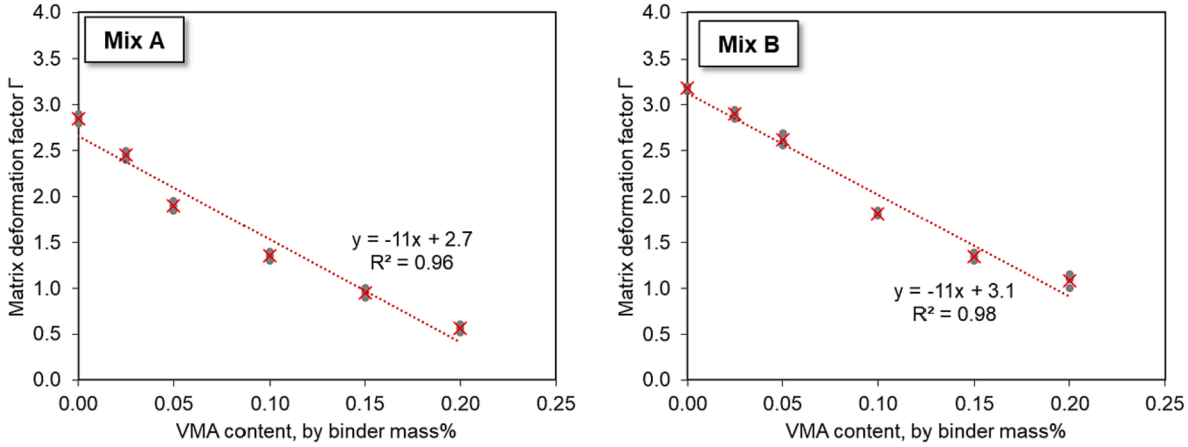

Fig. 7. Matrix deformation factor at various VMA contents.

3.2. Composite fresh properties

The flow table result shown in Fig. 9 suggests that the HPMC incorporation reduced ECC's workability as indicated by the deformation factor. A linear correlation can be established between the deformation factor and the VMA content for both mixes. Fig. 9 presents two datasets for each mix: the deformation factor measured with "no vibration" and "after vibration". The former was measured immediately after lifting the mini-slump cone, while the latter was measured after agitating the mixture by 25 drops of the flow table. The reference line indicates the reference PVA-ECC made with the same matrix but with 2 vol% PVA fiber.

Compared to PP fiber, PVA fiber is easy to mix into the cementitious matrix and forms a self-compacting behavior and a high flowability for typical PVA-ECC. Using PP fibers in place of PVA, however, resulted in a significant loss of workability by decreasing the deformation factor from 2.0 to 2.5 to below 1.0. The VMA incorporation further aggravates this trend, forming a nearly dry stiff mix when the VMA content exceeds 1.5 % for Mix A and 2.0 % for Mix B. Although the mixtures can be compacted by vibration, the fresh mixture appears to be thick and difficult for regular cast-in-place applications.

3.3. Fiber dispersion uniformity

*Fig. 10 shows that increasing the matrix plastic viscosity is conducive to PP fiber dispersion. As indicated in the example images shown in Fig. 11, the sample cross-section was segmented into 16 × 8 units, and the fluorescent objects were counted in each unit as the number of fibers

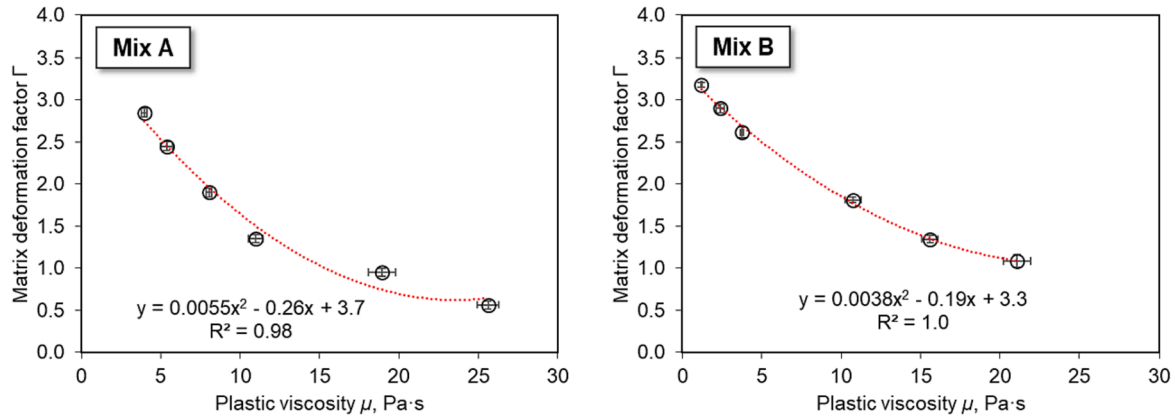

Fig. 8. Correlation between matrix plastic viscosity and deformation factor.

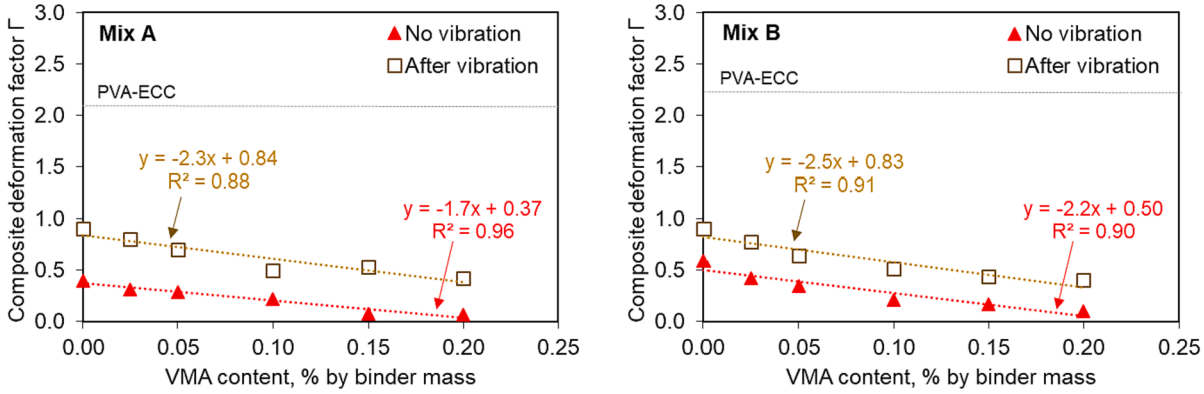

Fig. 9. Composite deformation factor versus VMA content.

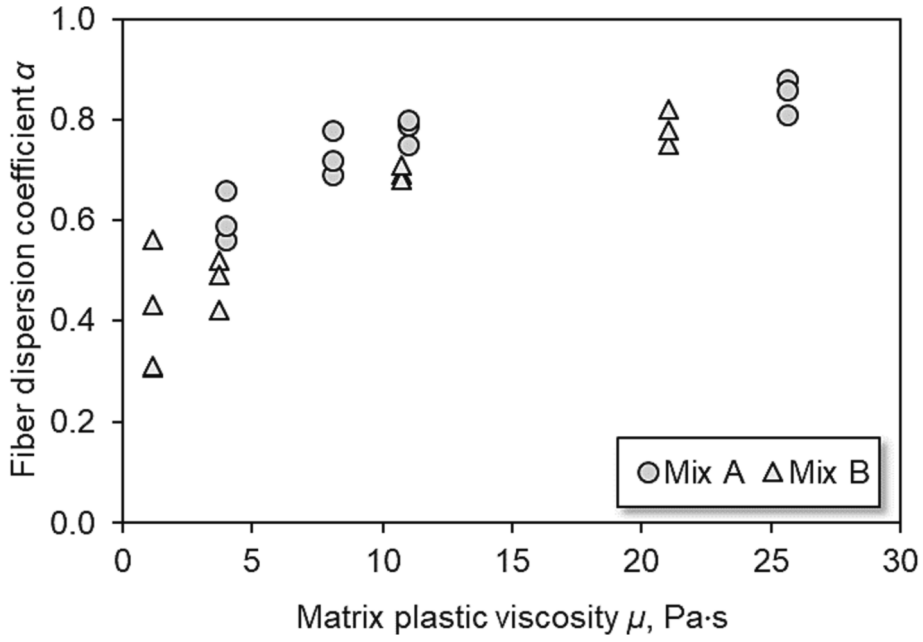

Fig. 10. Fiber dispersion coefficient at different levels of matrix plastic viscosity.

x_i. At comparable levels of matrix plastic viscosity, the fiber dispersion coefficient appears to be higher in Mix A than in Mix B, indicating that the presence of silica sand is potentially detrimental for PP fiber dispersion. As shown in Fig. 11, Mix B (Fig. 11**b**) exhibited local fiber agglomeration which led to a less uniform fiber distribution among the unit areas compared to Mix A (Fig. 11**a**). Previous studies [41,42] noted that introducing aggregates with a particle size larger than the fiber spacing accentuates the fiber clumping and interactions in the paste.

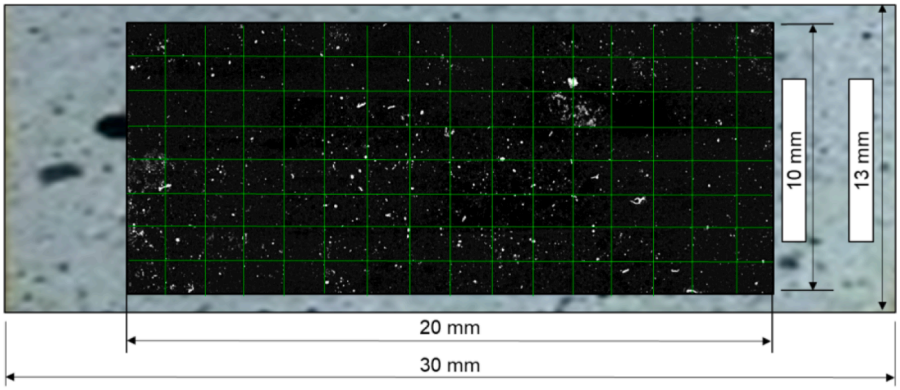

(a) Fiber dispersion for Mix A without sand

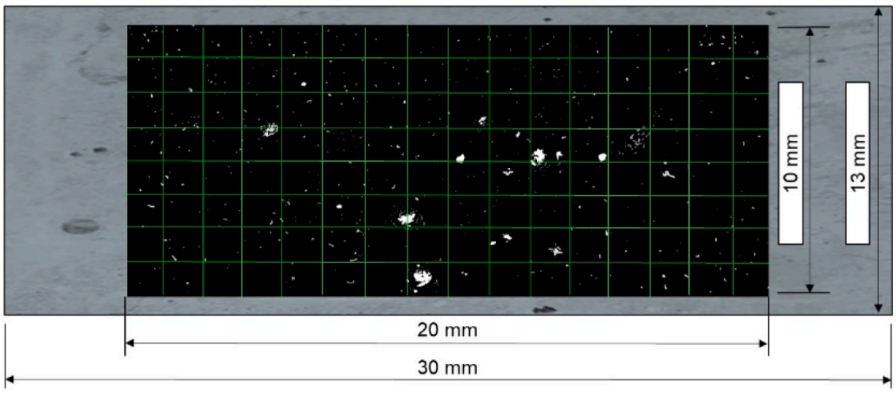

(b) Fiber dispersion for Mix B with sand

Fig. 11. Example microscopic images of sample sections.

This creates a non-uniform fiber distribution in the vicinity of the aggregate surface. Compared to typical PVA fibers used in conventional ECC, PP has a smaller diameter and thus a larger number of fibers on a unit cross-sectional area for the same fiber volume fraction. Hence, compared to PVA-ECC, PP-ECC possesses a smaller fiber spacing and a higher tendency to clump when sand is incorporated. This indicates that a mortar matrix with a reduced amount and/or size of sand is favorable for PP fiber dispersion.

3.4. Composite hardened properties

The mechanical test results suggest that there exists an optimal range of VMA dosage that maximizes the composite tensile strength and strain capacity. The tensile stress–strain curves are shown in Fig. 12 and Fig. 13 for Mix A and Mix B, respectively. All mixes exhibited distinct strain-hardening characteristics, with the ultimate tensile strength varying in 2.4–4.2 MPa for Mix A and 2.6–3.5 MPa for Mix B. The tensile strain capacity ranged from 1.8 to 4.6 % and 1.8 to 7.0 % for Mix A and Mix B, respectively. It suggests that sand incorporation increases the variability of tensile strength and strain capacity.

VMA has an evident influence on the composite tensile property. Fig. 14 illustrates the ultimate tensile strength and strain capacity as a function of the VMA content. By adding 0.1 % VMA, the composite tensile strength achieved the peak values at 4.2 MPa for Mix A and 3.5 MPa for Mix B. The corresponding tensile strain capacity reached 4.6 % and 6.3 % for the two mixes, respectively. The tensile strain capacity was improved by adding VMA up to 0.1 % for Mix A and 0.15 % for Mix B and was found to decrease by further increasing the VMA dosage. It seems that 0.1–0.15 % VMA was a desirable addition to simultaneously optimize the tensile strength and ductility. The corresponding matrix viscosity is approximately 11 Pa·s, slightly higher than that for PVA fiber, i.e., ~7 Pa·s [17]. At this viscosity level, Mix B exhibited a relatively higher strain capacity than Mix A due to the lower binder content and matrix cracking strength associated with the sand incorporation.

At a 0.2 % VMA dosage, the composite tensile ductility decreased substantially to 1.8 % for Mix A and 3.7 % for Mix B. On the fracture plane, large voids were identified, indicating poor compaction during casting (see Fig. 15). This behavior can be associated with the low flowability induced by the overdosed VMA, which increased the entrapped air and thus reduced the effective cross-sectional area and the number of fibers on the fracture plane. This effect of the HPMC incorporation was also identified by Fischer et al., [43], who reported an entrapped air content up to ~ 20 % with the air void size up to 10 mm. The air bubbles cannot escape due to the high cohesiveness of the mix and tend to reduce the ultimate tensile strength at high VMA contents. Note that the rheological properties vary with different types of VMA, and the matrix viscosity, rather than the actual dosage of VMA, should be tailored as the variable. Li and Li [17] reported that the PVA fiber dispersion and ECC tensile strain capacity could be improved by increasing the matrix viscosity up to 14.2 Pa·s. However, the ultimate tensile strength of PVA-ECC was found to decrease when the matrix viscosity exceeded ~ 7 Pa·s due to the entrapped air voids. For PP-ECC, as shown in Fig. 14, it is recommended to control the matrix viscosity at ~ 11 Pa·s (i.e., VMA content at ~ 0.1 % by binder mass) for optimal mechanical performance. The results of the present study suggest that, within an acceptable range of workability for casting and compaction, increasing the fiber dispersion (as indicated by α) can improve the PP-ECC's tensile strength and strain capacity.

The reduction of PP-ECC tensile strain capacity at high VMA contents observed in Fig. 14 can be associated with the flaw size distribution

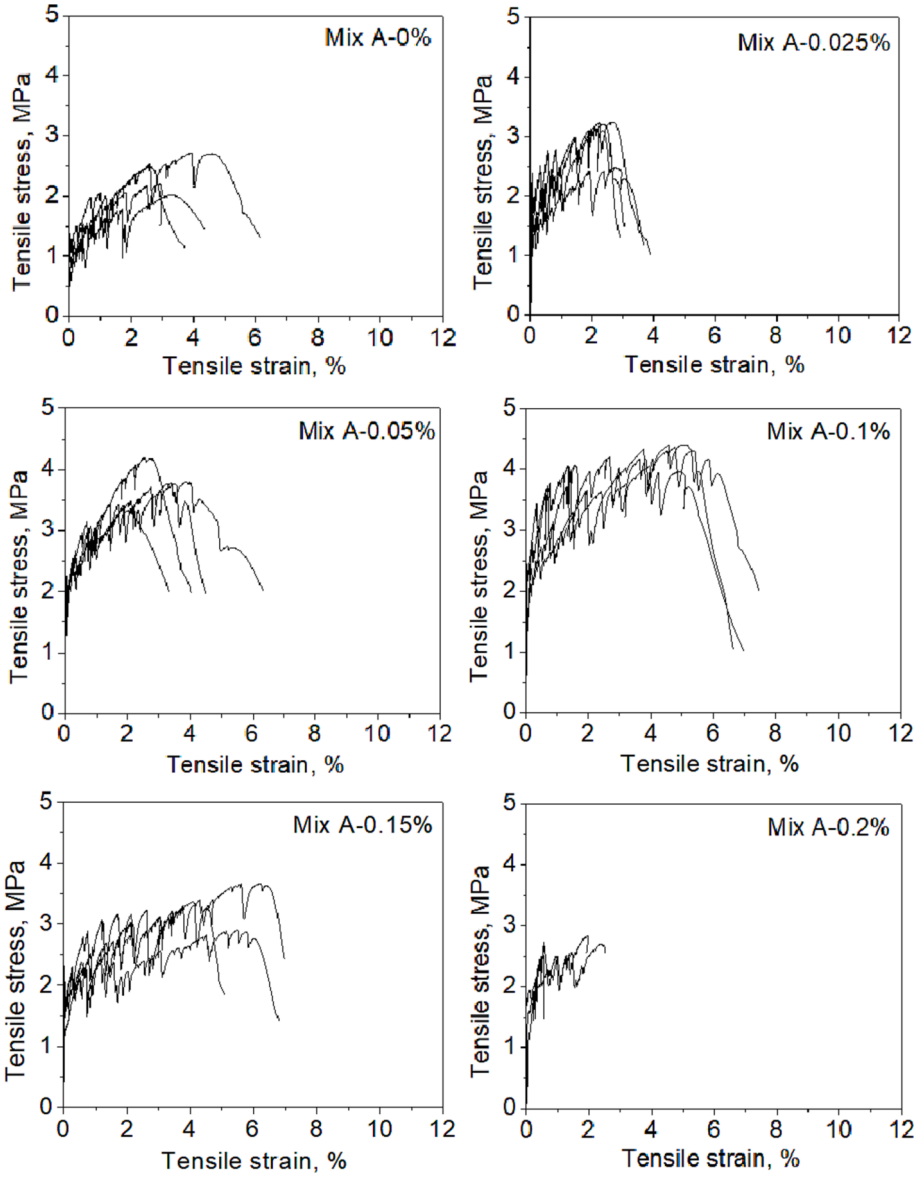

Fig. 12. Tensile stress–strain curves of Mix A PP-ECC at different VMA contents.

among different crack planes. The composite system must satisfy the stress and energy criteria in the ECC design framework to attain robust strain-hardening characteristics. Fig. 16 illustrates the fiber bridging σ-δ curve at a single crack opening [44,45]. Large voids induced by low workability tend to decrease the matrix steady-state first cracking strength σ_{ss} and fiber bridging capacity σ_0 at the crack location. Despite an improved fiber dispersion, poor compaction may reduce the uniformity of flaw size by entrapping large air voids (in millimeter size shown in Fig. 15b) within the specimen, and the existence of large voids could result in a significant reduction in the net cross-sectional area for fiber bridging and thus the local σ_0. The composite ultimate tensile strength is governed by the smallest σ_0 among crack planes along the specimen length and tends to decrease accordingly. The lowered σ_0 also increases the possibility of violating the stress criterion within the specimen, as more potential crack planes may have a cracking strength σ_{ss} higher than the lowest σ_0. The smaller flaws on these sections remain unactivated during the entire loading process, and the composite would develop an unsaturated crack pattern. Hence, the specimen tends to develop fewer cracks and lower composite ductility, as observed for Mix A-0.2 % and Mix B-0.2 %.

4. Conclusions

This study examines the relation between PP fiber distribution and the matrix viscosity and identifies the desirable level of matrix viscosity for ECC's fresh and hardened properties. An optimal range of matrix viscosity exists for maximizing PP-ECC's tensile strain capacity and ultimate tensile strength simultaneously. To achieve the designed fiber bridging capacity, a good dispersion of PP fibers is necessary, which requires a sufficient level of matrix viscosity. Increasing the matrix viscosity from ~ 1 to 26 Pa·s was found to improve PP-ECC fiber dispersion coefficient from 0.43 to 0.85. However, an overly viscous matrix lowers the workability of fresh mixtures, thus reducing the composite tensile strength and ductility by altering the flaw distribution, particularly by entrapping large air voids during mixing. In this study, the optimal level of matrix plastic viscosity was found to be ~ 11 Pa·s for PP fiber, which is higher than that for conventional PVA fiber, i.e., 7 Pa·s. This leads to the matrix deformation factors of 1.4 for PP-ECC without sand and 1.8 for PP-ECC with sand. By tailoring the matrix viscosity and PP fiber dispersion, the composite tensile strength and strain can be improved by 79 % and 292 %, respectively.

The matrix viscosity can be controlled effectively using HPMC as a

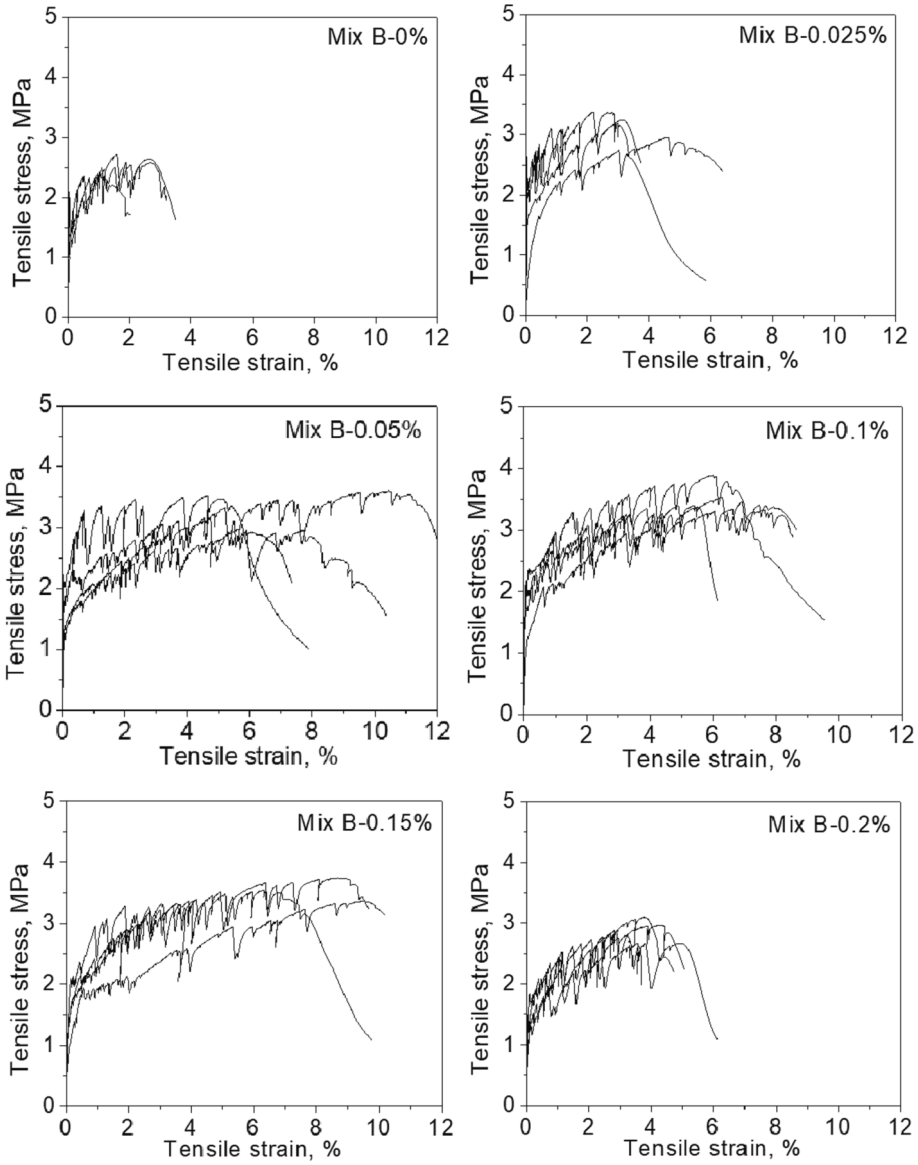

Fig. 13. Tensile stress–strain curves of Mix B PP-ECC at different VMA contents.

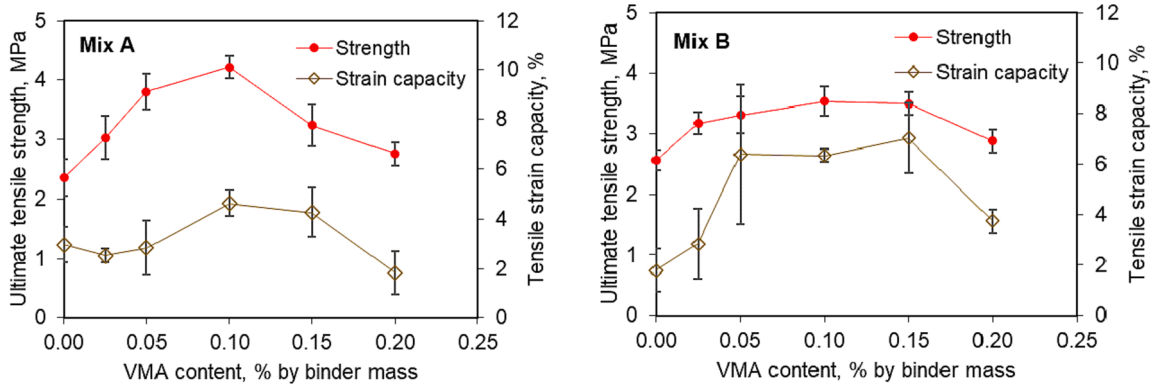

Fig. 14. PP-ECC tensile strength and strain capacity at varying VMA contents.

VMA. The matrix deformability measured by the mini-slump flow table can be correlated with the matrix viscosity and used as a simple indicator in practical PP-ECC design. Further investigation should address the impact of matrix viscosity on the flaw size and flaw distribution and the potential alterations of ECC's micromechanical properties, including matrix cracking strength, fracture toughness, and fiber/matrix interfacial bond. PP fiber dispersion may also be examined in other ECC binder systems based on ordinary Portland cement, and the individual and

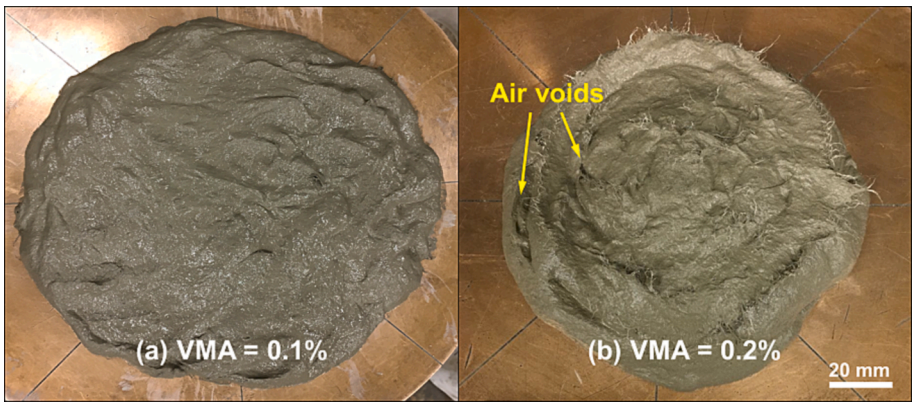

Fig. 15. Typical appearance of fresh PP-ECC mixture with 0.1% and 0.2% VMA by binder mass.

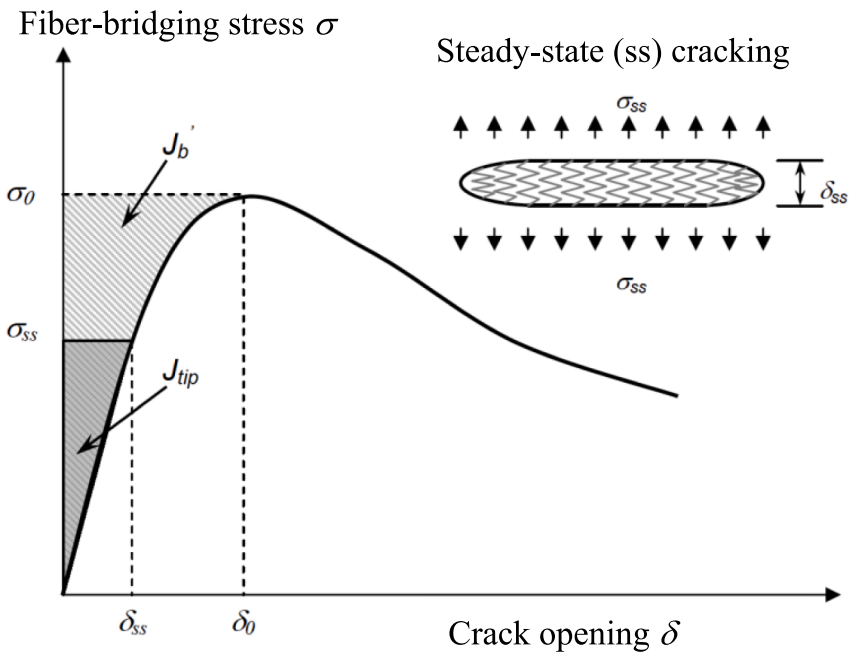

Fig. 16. ECC fiber bridging stress σ – crack opening δ curve [44,45].

coupling effects of each cementitious component (such as limestone and metakaolin) on fiber dispersion warrant further studies.

CRediT authorship contribution statement

Duo Zhang: Validation, Formal analysis, Investigation, Writing – original draft. **He Zhu:** Validation, Formal analysis, Investigation. **Menjun Hou:** Validation, Formal analysis, Investigation. **Kimberly E. Kurtis:** Supervision, Writing – review & editing. **Paulo J.M. Monteiro:** Supervision, Writing – review & editing. **Victor C. Li:** Supervision, Writing – review & editing, Project administration, Funding acquisition.

Declaration of Competing Interest

The authors declare that they have no known competing financial interests or personal relationships that could have appeared to influence the work reported in this paper.

Data availability

Data will be made available on request.

Acknowledgment

The authors are grateful for the funding support by the US Department of Energy ARPA-e (award No. DE-AR0001141) to the University of Michigan.

References

[1] Li, V.C., Engineered Cementitious Composites (ECC): Bendable Concrete for Sustainable and Resilient Infrastructure. 2019: Springer.
[2] V.C. Li, Tailoring ECC for special attributes: A review, Int. J. Concr. Struct. Mater. 6 (3) (2012) 135–144.
[3] S. Wang, Micromechanics based matrix design for Engineered Cementitious Composites, University of Michigan, Ann Arbor, 2005. Ph.D. Dissertation.
[4] S. Wang, V.C. Li, Engineered cementitious composites with high-volume fly ash, ACI Mater. J. 104 (3) (2007) 233.
[5] H. Liu, Q. Zhang, C. Gu, H. Su, V.C. Li, Influence of micro-cracking on the permeability of engineered cementitious composites, Cem. Concr. Compos. 72 (2016) 104–113.
[6] M.D. Lepech, V.C. Li, Water permeability of engineered cementitious composites, Cem. Concr. Compos. 31 (10) (2009) 744–753.
[7] H. Liu, Q. Zhang, C. Gu, H. Su, V. Li, Influence of microcrack self-healing behavior on the permeability of engineered cementitious composites, Cem. Concr. Compos. 82 (2017) 14–22.

[8] E.N. Herbert, V.C. Li, Self-healing of microcracks in Engineered Cementitious Composites (ECC) under a natural environment, Materials 6 (7) (2013) 2831–2845.
[9] V.C. Li, E.H. Yang, Self healing in concrete materials, Springer, Dordrecht, Self-Healing Materials, 2007, pp. 161–193.
[10] H. Liu, Q. Zhang, V. Li, H. Su, C. Gu, Durability study on engineered cementitious composites (ECC) under sulfate and chloride environment, Constr. Build. Mater. 133 (2017) 171–181.
[11] Li, V.C., Engineered cementitious composites (ECC) material, structural, and durability performance. 2008. In *Concrete Construction Engineering Handbook*, Chapter 24, pp24-1 to 24-40, Ed. E. Nawy, published by CRC Press, 2008.
[12] M. Lepech, V.C. Li, Durability and long term performance of engineered cementitious composites. in Proceedings of the international Workshop on HPFRCC in Structural Applications, 2005.
[13] Li, M., R. Ranade, L. Kan, and V.C. Li, On improving the infrastructure service life using ECC to mitigate rebar corrosion. 2nd International Symposium on Service Life Design for Infrastructure. Paris, France, 2010: p. 773–782.
[14] E.-H. Yang, V.C. Li, Strain-hardening fiber cement optimization and component tailoring by means of a micromechanical model, Constr. Build. Mater. 24 (2) (2010) 130–139.
[15] Yang, E.H. and V.C. Li, A Micromechanical model for fiber cement optimization and component tailoring. 10th International Inorganic-Bonded Fiber Composites Conference, Sao Paulo, Brazil, 2006.
[16] V.C. Li, Engineered cementitious composites (ECC) - tailored composites through micromechanical modeling, in: N. Banthia, A. Bentur, A.A. Mufti (Eds.), Fiber Reinforced Concrete Present and Future, Canadian Society for Civil Engineering, Montreal (Canada), 1997, pp. 64–97.
[17] M. Li, V.C. Li, Rheology, fiber dispersion, and robust properties of engineered cementitious composites, Mater. Struct. 46 (3) (2013) 405–420.
[18] W. Si, M. Cao, L. Li, Establishment of fiber factor for rheological and mechanical performance of polyvinyl alcohol (PVA) fiber reinforced mortar, Constr. Build. Mater. 265 (2020), 120347.
[19] M. Cao, W. Si, C. Xie, Relationship of rheology, fiber dispersion, and strengths of polyvinyl alcohol fiber-reinforced cementitious composites, ACI Mater. J. 117 (3) (2020) 191–204.
[20] E.-H. Yang, Designing added functions in engineered cementitious composites, University of Michigan, Ann Arbor, 2008. Ph.D. Thesis.
[21] B. Felekoglu, K. Tosun-Felekoglu, R. Ranade, Q. Zhang, V.C. Li, Influence of matrix flowability, fiber mixing procedure, and curing conditions on the mechanical performance of HTPP-ECC, Compos. B Eng. 60 (2014) 359–370.
[22] B. Felekoğlu, K. Tosun-Felekoğlu, E. Gödek, A novel method for the determination of polymeric micro-fiber distribution of cementitious composites exhibiting multiple cracking behavior under tensile loading, Constr. Build. Mater. 86 (2015) 85–94.
[23] S.S. Berriel, A. Favier, E.R. Domínguez, I.S. Machado, U. Heierli, K. Scrivener, F. M. Hernández, G. Habert, Assessing the environmental and economic potential of limestone calcined clay cement in cuba, J. Cleaner Prod. 124 (2016) 361–369.
[24] Y. Dhandapani, T. Sakthivel, M. Santhanam, R. Gettu, R.G. Pillai, Mechanical properties and durability performance of concretes with Limestone Calcined Clay Cement (LC3), Cem. Concr. Res. 107 (2018) 136–151.
[25] K. Scrivener, F. Martirena, S. Bishnoi, S. Maity, Calcined clay limestone cements (LC3), Cem. Concr. Res. 114 (2018) 49–56.
[26] H. Zhu, D. Zhang, T. Wang, H. Wu, V.C. Li, Mechanical and self-healing behavior of low carbon engineered cementitious composites reinforced with PP-fibers, Constr. Build. Mater. 259 (2020), 119805.
[27] J. Liu, W. Zhang, Z. Li, H. Jin, W. Liu, L. Tang, Investigation of using limestone calcined clay cement (LC3) in engineered cementitious composites: the effect of propylene fibers and the curing system, J. Mater. Res. Technol. 15 (2021) 2117–2144.
[28] N. Nair, K.M. Haneefa, M. Santhanam, R. Gettu, A study on fresh properties of limestone calcined clay blended cementitious systems, Constr. Build. Mater. 254 (2020), 119326.
[29] S. Ferreiro, D. Herfort, J. Damtoft, Effect of raw clay type, fineness, water-to-cement ratio and fly ash addition on workability and strength performance of calcined clay–limestone Portland cements, Cem. Concr. Res. 101 (2017) 1–12.
[30] K. Scrivener, F. Avet, H. Maraghechi, F. Zunino, J. Ston, W. Hanpongpun, A. Favier, Impacting factors and properties of limestone calcined clay cements (LC3), Green Mater. 7 (1) (2018) 3–14.
[31] M.D. Lepech, V.C. Li, Large-scale processing of engineered cementitious composites, ACI Mater. J. 105 (4) (2008) 358.
[32] B.Y. Lee, J.-K. Kim, J.-S. Kim, Y.Y. Kim, Quantitative evaluation technique of Polyvinyl Alcohol (PVA) fiber dispersion in engineered cementitious composites, Cem. Concr. Compos. 31 (6) (2009) 408–417.
[33] J.-K. Kim, J.-S. Kim, G.J. Ha, Y.Y. Kim, Tensile and fiber dispersion performance of ECC (engineered cementitious composites) produced with ground granulated blast furnace slag, Cem. Concr. Res. 37 (7) (2007) 1096–1105.
[34] H. Paiva, L. Esteves, P. Cachim, V. Ferreira, Rheology and hardened properties of single-coat render mortars with different types of water retaining agents, Constr. Build. Mater. 23 (2) (2009) 1141–1146.
[35] D.G. Soltan, V.C. Li, A self-reinforced cementitious composite for building-scale 3D printing, Cem. Concr. Compos. 90 (2018) 1–13.
[36] L. Patural, P. Marchal, A. Govin, P. Grosseau, B. Ruot, O. Deves, Cellulose ethers influence on water retention and consistency in cement-based mortars, Cem. Concr. Res. 41 (1) (2011) 46–55.
[37] M. Westerholm, B. Lagerblad, J. Silfwerbrand, E. Forssberg, Influence of fine aggregate characteristics on the rheological properties of mortars, Cem. Concr. Compos. 30 (4) (2008) 274–282.
[38] C. Liu, X. Wang, Y. Chen, C. Zhang, L. Ma, Z. Deng, C. Chen, Y. Zhang, J. Pan, N. Banthia, Influence of hydroxypropyl methylcellulose and silica fume on stability, rheological properties, and printability of 3D printing foam concrete, Cem. Concr. Compos. 122 (2021), 104158.
[39] B. Ma, Y. Peng, H. Tan, S. Jian, Z. Zhi, Y. Guo, H. Qi, T. Zhang, X. He, Effect of hydroxypropyl-methyl cellulose ether on rheology of cement paste plasticized by polycarboxylate superplasticizer, Constr. Build. Mater. 160 (2018) 341–350.
[40] Y. Chen, S.C. Figueiredo, Z. Li, Z. Chang, K. Jansen, O. Çopuroğlu, E. Schlangen, Improving printability of limestone-calcined clay-based cementitious materials by using viscosity-modifying admixture, Cem. Concr. Res. 132 (2020), 106040.
[41] D. De Koker, G. Van Zijl, Extrusion of engineered cement-based composite material, Proceedings of BEFIB (2004) 1301–1310.
[42] M. Sahmaran, M. Lachemi, K.M. Hossain, R. Ranade, V.C. Li, Influence of aggregate type and size on ductility and mechanical properties of engineered cementitious composites, ACI Mater. J. 106 (3) (2009) 308.
[43] G. Fischer, W. Shuxin, Design of engineered cementitious composites (ECC) for processing and workability requirements, in: Brittle Matrix Composites 7, Elsevier, 2003, pp. 29–36.
[44] V.C. Li, S. Wang, C. Wu, Tensile strain-hardening behavior of polyvinyl alcohol engineered cementitious composite (PVA-ECC), ACI Materials Journal-American Concrete Institute 98 (6) (2001) 483–492.
[45] E.-H. Yang, Y. Yang, V.C. Li, Use of high volumes of fly ash to improve ECC mechanical properties and material greenness, ACI Mater. J. 104 (6) (2007) 620.